Bloch mode analysis of subwavelength polarizing planar optics

Raphaël Mulin, François Deneuville, Olivier Jeannin, Matthieu Boffety, Jerome Vaillant

Bloch mode analysis of subwavelength polarizing planar optics

R. Mulin*[a], F. Deneuville[b], O. Jeannin[a], M. Boffety[c], J. Vaillant[b]
[a]STMicroelectronics, 38920, Crolles, France;
[b]Univ. Grenoble Alpes, CEA, LETI, 38000, Grenoble, France;
[c]Univ. Paris-Saclay, Institut d'Optique Graduate School, CNRS, Laboratoire Charles Fabry, 91127, Palaiseau, France

ABSTRACT

The purpose of this paper is to investigate the impact of advanced immersion lithography process for the development of polarization optics at pixel level on CMOS image sensors. In the first part of this paper, we use Bloch formalism to define regimes that depend on the number of propagative Bloch modes within the structure. The presented analysis gives estimations of required features size to operate in NIR and visible range. The second part of this paper present optical characterization of silicon lamellar grating made on 300 mm wafer using advanced immersion lithography. Characterization results are discussed with respect to optical simulations and reconstructed grating profile is compared to patterning features estimated during first part.

Keywords: Bloch modes, RCWA, polarization, subwavelength optics, CMOS image sensor.

1. INTRODUCTION

Emerging imaging vision applications, such as medical diagnosis, target detection, reflection removal during post-processing of photography images or 3D detection enhancement [1,2], require polarization sensitive imagers. Thanks to their abilities to be miniaturized and highly transmissive, pixelated subwavelength structuration is a promising way to achieve optical functionality in CMOS image sensor. Main strategies to bring pixels sensitive to polarization consist in high contrast grating acting as reflective polarizer. [3,4].

The paper is organized as follow: in section 2 we develop a Bloch mode analysis on grid structure to define the different regimes and feature size suitable for polarizer filter in near infrared and visible range. In section 3 we present demonstration of grid with a period of 100 nm realized using CMOS compatible immersion lithography and compare experimental polarization dependent reflection to simulation. We conclude in section 4 with the opportunities offered by this demonstration to realize pixel-level polarizers.

2. BLOCH MODES IN GRATINGS

2.1 Geometry of the grating

The structures considered in this paper are based on metasurface process developed in CEA-LETI on STMicroelectronics image sensors. These metasurfaces aim to work in near-infrared range, at 940nm, and are based on nano-structured amorphous silicon embedded in silicon dioxide. These materials offer high refractive index contrast with negligible absorption [5-7].

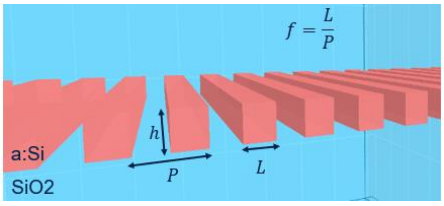

Figure 1. Grating Geometry

The geometry of the grating is shown in Figure 1. The period of the grating is denoted *P*, the bar cross section is defined by its height *h* and their width *L*, and we define the fill-factor *f* as the ratio of *L* over *P*. The bars are considered infinite in the other direction.

2.2 High contrast grating

High contrast grating achieves 100 % reflection and can therefore be used to filter light [8,9]. Transmission of the grating is computed with Reticolo [10] and plotted for both polarizations TE and TM in Figure 2. Colormaps brings out three optical behaviors depending on grating period. For short period (P < 300nm), the grating provides high transmission with low variation. For period larger than λ/n_{sio2} (650nm), the grating is diffracting. Between those two regions, the grating transmission can reach 0 or 1, and is very sensitive to grating geometry. Some parameter sets allow for polarizer operation at normal incidence, i.e., reflecting one component and transmitting the other.

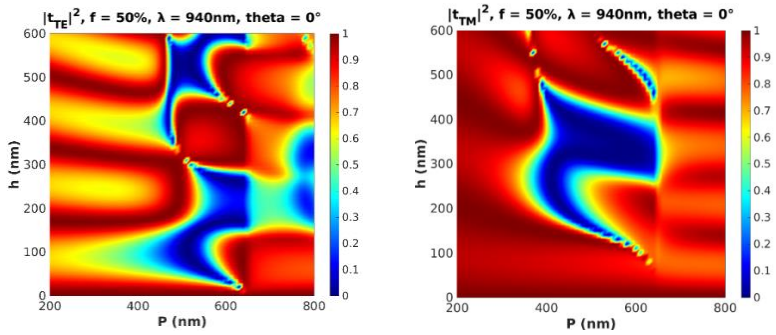

Figure 2. Transmission colormaps for TE polarization (left) and Transmission for TM polarization (right).

2.3 Bloch mode analysis

Operation principles of subwavelength element rely on electric field condition at interfaces, which imposes that only particulars wave shapes can exist inside the nano-structuration. Referred as "Bloch modes" [11], those shapes can be associated to a propagation constant and to an optical index. This analysis is particularly convenient because it doesn't depend on height for straight geometry. These modes can be computed for any geometry, using Rigorous Coupled Wave Analysis (RCWA) method. Figure 3 and Figure 4, generated with Reticolo, show the effective indices of Bloch modes for a 50 % fill factor grating. The fundamental mode index (TE0 - blue curves) is real regardless the period, resulting in propagation through the structure without attenuation. Effective indexes of non-fundamental modes change from pure imaginary to real as the period increases, this is the mode cut-off [8]. This means these switches from evanescent waves to propagative waves. First mode cut-off distinguishes if the grating will behave as a waveguide (only one propagative mode) or as a resonant element (more than one mode is propagative). "Waveguiding" operation shows better efficiency, tolerance to grating parameters and incidence angle [12]. Therefore, the geometry associated with first mode cut-off mode should be taken as critical dimensions to be achieved.

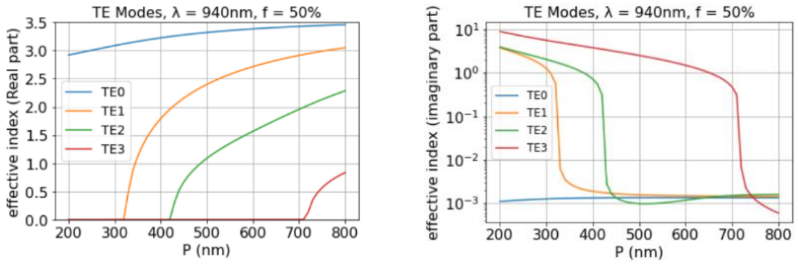

Figure 3. Effective refractive index (left) and effective extinction coefficient (right) for TE polarization.

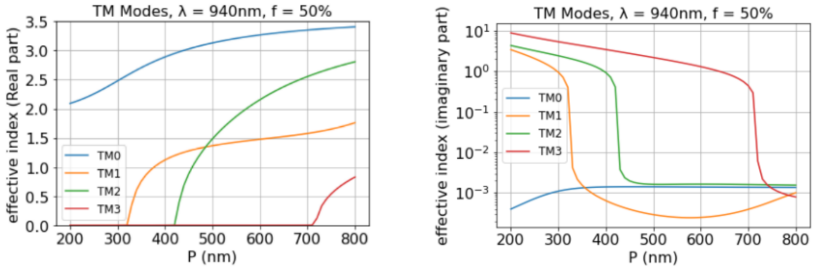

Figure 4. Effective refractive index (left) and effective extinction coefficient (right) for TM polarization.

2.4 Critical dimension for controlling the wavefront in IR and visible

Figure 5 plots the number of propagating modes as a function of grating parameters (up to four modes) and shows the entire parameter space for a particular wavelength. We founded exact same graph for both polarizations. For a fill factor of 50 %, one can report mode cut-off period of two first non-fundamental modes in Figure 2 to Figure 4. At a wavelength of 940 nm, for period bellow 250 nm, the grating behaves as a waveguide element regardless of the fill factor.

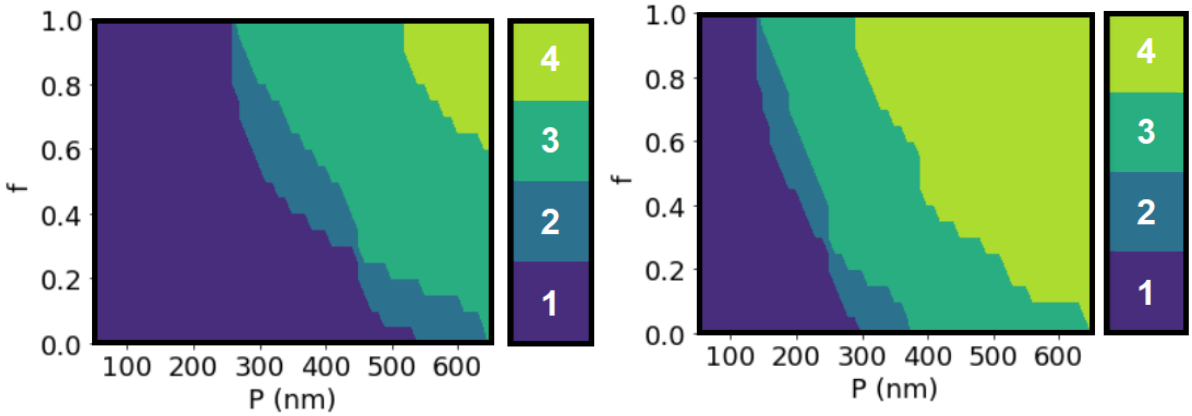

Figure 5. Number of propagating modes at λ = 940 nm (left) and λ = 550nm (right).

For shorter wavelength, it is expected that geometries associated with mode cut-off are smaller. On the right side of Figure 5 is plotted the number of propagative modes for a 550 nm wavelength. Required period to make the grating behaving as a waveguide is now between of 120 nm and 300 nm depending on fill factor.

Another important contribution to the change between left and right part of Figure 5 is the refractive index variation of silicon. It is noteworthy that silicon is an absorptive material for visible light. As a consequence, height and fill factor should be limited to minimize losses.

3. EXEPERIMENTAL GRATING

3.1 Component description

In order to investigate the capability to create small structures on CMOS image sensors, we create gratings on 300 mm crystalline silicon wafers using immersion lithography.

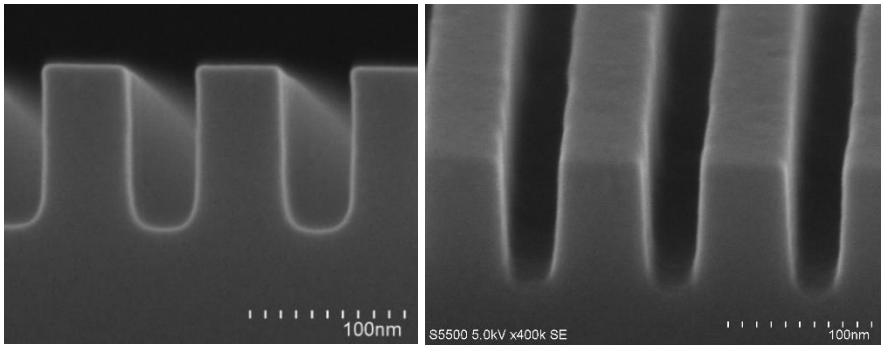

Figure 6. Grating microscopy.

Figure 6 present electronic microscopic microscopy imaging image of silicon grating made using advanced lithography process of CEA-LETI. Crystalline silicon is directly etched on 300 mm wafer. We achieve a The period *P* of 100 nm, a silicon wire width *L* of 50 nm (fill-factor *f* = 50 %) and the height *h* of 100 nm. We can notice a in light gray thin dioxide of silicon which is naturally created during contact with air.

3.2 Process description

For this demonstrator, we start with bare 300 mm crystalinne silicon wafers. A first step of lithography consists of spin-coat deposition of ultra-violet (λ = 193 nm) photosensitive resin compatible with immersion lithography scanner. Then this resin is exposed with bar pattern (50 nm width, 50 nm space) and developed. Then the silicon is dry-etched to transfer the resin footprint into the silicon. The depth to pattern is controlled by the duration of the etch. Finally the resin residues are stripped and the wafer are cleanned, creating a thin silicon dioxide layer at the silicon surface seen as a light gray line on the surface of the silicon on Figure 6. This process is very close to the one developped for metasurface, and thus will be compatible with two-dimensional structuration and amorphous silicon etching on SiO_2 substrate. In the case of etching silicon on a dioxide silicon substrate, the height is defined by the amorphous silicon deposition. In addition, the present rounding corner we can see on Figure 6 at the bottom of the grating, will not appear thanks to the etching selectivity between amorphous silicon and silicon dioxide.

3.2 Experimental setup

We optically characterized the grating in CEA-LETI clean room. Polarimetric-reflectometry measurements were acquired for different polarization angle θ_p, incidence angle θ_i, and azimuthal angle θ_r, experimental setup is resume by figure 8.

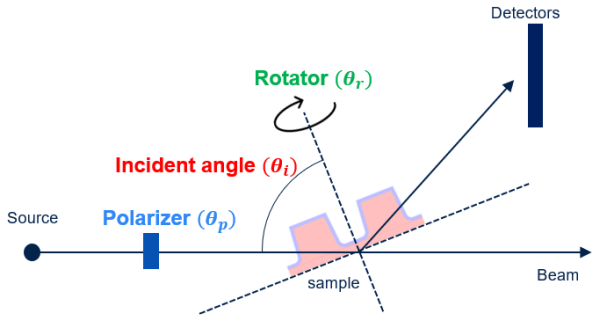

Figure 7. Experimental setup.

We took 50 measurements at different grating locations for wavelength in visible and near infrared range, this enables to estimate the sample non-uniformity and measurement system instability. We calculated standard deviation of the measurements with equation 1.

$$\sigma^2 = \frac{1}{N-1}\sum_{i=1}^{N}(x_i - \mu)^2 \quad (1)$$

Where σ is the standard deviation of our data and is of the order of 10^{-3}. Data obtained for θ_p = 90°, θ_i = 55° and θ_r = 90°, are plotted in figure 8. The blue band show the 3 standard deviation interval.

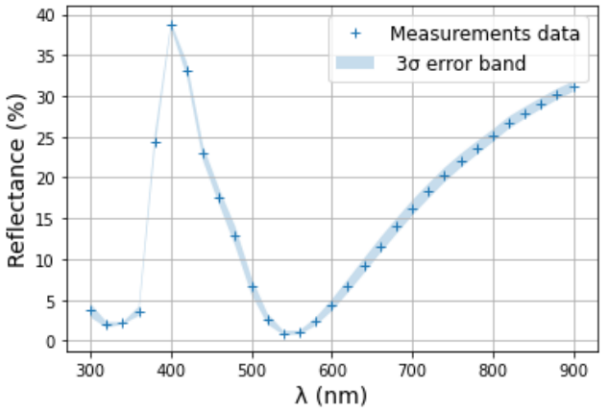

Figure 8. Experimental data.

3.3 Results and model fitting

Optical simulations were performed to estimate the grating reflectance spectrum. Figure 9 describes parameters we used to simulate the grating geometry. Gradient-base minimization of χ^2 merit function is performed to reconstruct grating profile.

$$\chi^2 = \sum_{\lambda=300\text{nm}}^{\lambda=900\text{nm}} \frac{(R_{Exp}(\lambda) - R_{RCWA}(\lambda))^2}{\sigma_\lambda^2} \quad (2)$$

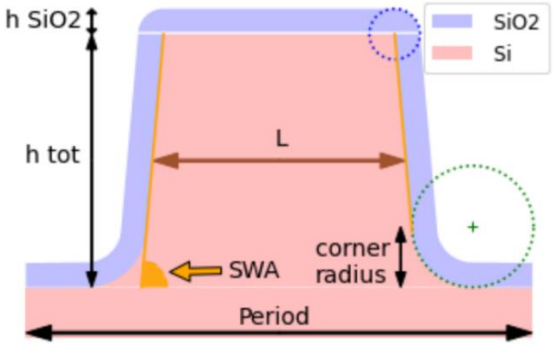

Figure 9. Grating simulation.

Figure 10 offers a comparison between curves obtained when fitting all parameters presented in Figure 10 with a simpler model (with parameters "SWA" and "corner radius" fixed to 90° and 0 nm). Results clearly shows that the simpler model is not able to reproduce the reflectance spectrum while the second parametrization fits experimental data inside confidence interval.

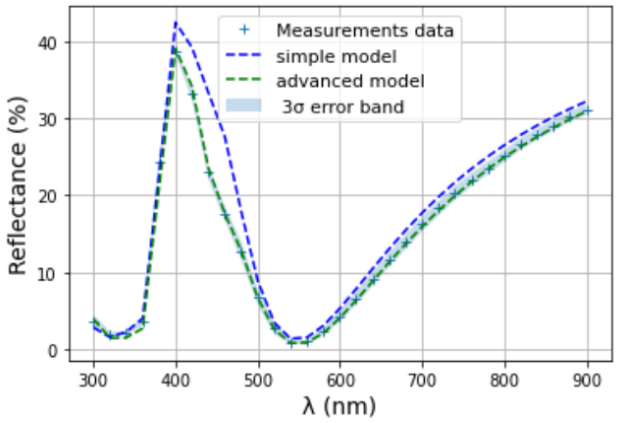

Figure 10. Comparison between data (cross), best fitted simple model (dashed blue line) and the best fitted advanced model (dash green line).

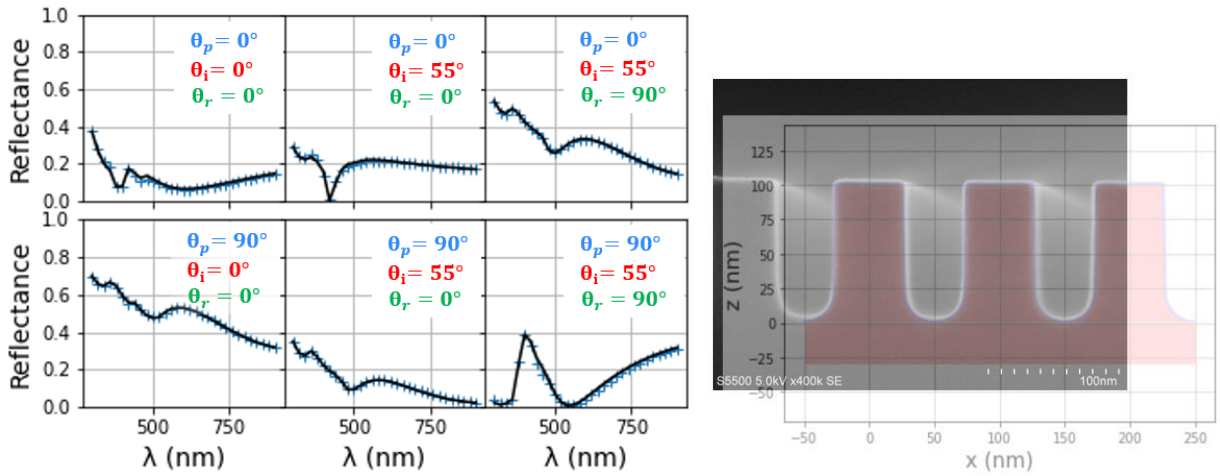

Figure 11. Fitted data with same parameter set (left) and reconstructed grating profile (right).

Data were obtained for six setup configurations and all of them were fitted with a unique set of parameters. Figure 11 shows the result of the optimization and table 1 the optimal parameters. This approach allows to fit the curves with fidelity. On the right side of Figure 11 comparison of the microscopy and reconstructed profile (with same scale) is shown, confirming that the range of optimized parameters gives an accurate description of the realized grating. Table 1 present fitted parameters.

Table 1. Optimal parameter set to fit the data.

P - Period (nm)	100
h - Height (nm)	103
L - Width (nm)	51
h SiO2- SiO_2 height (nm)	1.90
SWA (°)	89
Corner radius (nm)	26

4. CONCLUSION

We investigated industrialize solutions to bring CMOS pixels sensitive to polarization. Critical dimensions for controlling the wavefront can be estimated from Bloch mode analysis and we derived those features for NIR and visible. With the use of immersion lithography, we demonstrated access to critical feature size estimated in first part and this process is adaptable to more complex geometry on CMOS image sensors. Designs of planar optics providing multifunctionality and high performances leaves us optimistic about the potential of their development.

ACKNOWLEDGEMENT

Authors want to specially thank Olivier Dubreuil, Cédric Giroud-Garampon and Guido Rademaker for helping during realization, characterization, and microscopic imaging of the presented grating. We also acknowledge people working at STM and CEA-LETI involve in this study.

REFERENCES

[1] B. Varin, J. Rehbinder, J. Dellinger, C. Heinrich, J. Schmidt, C. Spenlén, D. Bagnard, and J. Zallat. "Tumor growth monitoring using polarized light," Proc. of Novel Biophotonics Techniques and Applications (2019). DOI:10.1117/12.2527020

[2] A. Kadambi, V. Taamazyan, B. Shi, and R. Raskar. "Polarized 3D: High-Quality Depth Sensing with Polarization Cues," Proc. of IICV (2015). DOI:10.1109/ICCV.2015.385

[3] K. J. Lee, J. Giese, L. Ajayi, R. Magnusson, and E. Johnson, "Resonant dielectric-grating polarizers for normal incidence operation," Proc. of IEEE Photonic Conference (2012). DOI:10.1109/IPCON.2012.6358558

[4] Chong Z., J. Hu, Y. Dong, A. Zeng, H. Huang, and C. Chong Zhang, "High efficiency all-dielectric pixelated metasurface for near-infrared full-Stokes polarization detection," Photon. Res. 9, 583-589 (2019). DOI:10.1364/PRJ.415342

[5] J. Vaillant et al., « SPAD array sensitivity improvement by diffractive microlens », IISW proceedings (2019)

[6] L. Dilhan, J. Vaillant, A. Ostrovsky, L. Masarotto, C. Pichard, et R. Paquet, « Planar microlenses for near infrared CMOS image sensors », Electron. Imaging, vol. 2020, no 7 (2021). DOI:10.2352/ISSN.2470-1173.2020.7.ISS-144.

[7] L. Dilhan et al., « Planar microlenses applied to SPAD pixels », IISW proceedings (2021).

[8] V. Karagodsky, F. G. Sedgwick, and C. J. Chang-Hasnain, "Theoretical analysis of subwavelength high contrast grating reflectors," Opt. Express 18, 16973-16988 (2010). DOI: 10.1364/OE.18.016973

[9] S. Villenave, S. Monfray, H. Benysty, Q. Abadie et. al., "Advanced Optic Filtering Based on Si Nanodisk Integration on 300 mm Glass Wafer," in Conference on Lasers and Electro-Optics, Technical Digest Series (2021). DOI:10.1364/CLEO_AT.2022.JW3A.41

[10] J.-P. Hugonin, P. Lalanne. (2021). Light-in-complex-nanostructures/RETICOLO: V9 (Version 9a). Zenodo. DOI:10.5281/zenodo.5905381.

[11] P. Lalanne, J. P. Hugonin and P. Chavel, "Optical properties of deep lamellar Gratings: A coupled Bloch-mode insight," in Journal of Lightwave Technology, vol. 24, no. 6, (2006). DOI:10.1109/JLT.2006.874555.

[12] C. Gigli, Q. Li, P. Chavel, G. Leo, M. Brongersma, P. Lalanne, "Fundamental limitations of Huygens' metasurfaces for optical beam shaping," Laser & Photonics Reviews, 15, 2000448 (2021). DOI:10.1002/lpor.202000448